Journal of Oral Microbiology

co-action PUBLISHING

ORIGINAL ARTICLE

VEGFR-2 reduces while combined VEGFR-2 and -3 signaling increases inflammation in apical periodontitis

Anca Virtej[1]*, Panagiota Papadakou[1], Hajime Sasaki[2], Athanasia Bletsa[3] and Ellen Berggreen[1]

[1]Department of Biomedicine, University of Bergen, Bergen, Norway; [2]Department of Immunology and Infectious Diseases, The Forsyth Institute, Cambridge, MA, USA; [3]Department of Clinical Dentistry, University of Bergen, Bergen, Norway

Background: In apical periodontitis, oral pathogens provoke an inflammatory response in the apical area that induces bone resorptive lesions. In inflammation, angio- and lymphangiogenesis take place. Vascular endothelial growth factors (VEGFs) and their receptors (VEGFRs) are key players in these processes and are expressed in immune cells and endothelial cells in the lesions.

Objective: We aimed at testing the role of VEGFR-2 and -3 in periapical lesion development and investigated their role in lymphangiogenesis in the draining lymph nodes.

Design: We induced lesions by pulp exposure in the lower first molars of C57BL/6 mice. The mice received IgG injections or blocking antibodies against VEGFR-2 (anti-R2), VEGFR-3 (anti-R3), or combined VEGFR-2 and -3, starting on day 0 until day 10 or 21 post-exposure.

Results: Lesions developed faster in the anti-R2 and anti-R3 group than in the control and anti-R2/R3 groups. In the anti-R2 group, a strong inflammatory response was found expressed as increased number of neutrophils and osteoclasts. A decreased level of pro-inflammatory cytokines was found in the anti-R2/R3 group. Lymphangiogenesis in the draining lymph nodes was inhibited after blocking of VEGFR-2 and/or -3, while the largest lymph node size was seen after anti-R2 treatment.

Conclusions: We demonstrate an anti-inflammatory effect of VEGFR-2 signaling in periapical lesions which seems to involve neutrophil regulation and is independent of angiogenesis. Combined signaling of VEGFR-2 and -3 has a pro-inflammatory effect. Lymph node lymphangiogenesis is promoted through activation of VEGFR-2 and/or VEGFR-3.

Keywords: *bone resorption*; *osteoclasts*; *angiogenesis and lymphangiogenesis*; *immune cells*; *cytokines*

*Correspondence to: Anca Virtej, Department of Biomedicine, University of Bergen, Jonas Lies Vei 91, NO-5009 Bergen, Norway, Email: anca.virtej@uib.no

Received: 31 May 2016; Revised: 15 August 2016; Accepted: 16 August 2016; Published: 19 September 2016

Apical periodontitis, a common inflammatory disease characterized by bone resorption, is mainly caused by the interaction of bacteria penetrating the root canal system with the host's immune response having the ultimate goal of restricting the infection to the root canal (1).

Key players in the inflammatory periapical responses are endothelial cells, polymorphonuclear leukocytes (PMNs), macrophages, lymphocytes, and bone resorptive cells, the osteoclasts, all of which contribute with the production of cytokines. Bacteria stimulate the production of pro-inflammatory cytokines in the lesions, particularly interleukin-1 (IL-1), tumor necrosis factor α (TNF-α), or receptor activator of nuclear factor kappa-B ligand (RANKL) (2, 3). TNF-α can stimulate osteoclastogenesis independently, whereas other cytokines like IL-1β trigger RANKL expression, that leads to osteoclast formation and activity (4). Animal studies have shown that some cytokines, like interferon γ (IFN-γ), IL-6, and IL-10, may exhibit an anti-inflammatory effect against periapical bone resorption (5, 6).

During inflammation, growth of blood and lymphatic vessels takes place, known as angio- and lymphangiogenesis, respectively (7). The signaling molecules with key involvement in these processes are vascular endothelial growth factor (VEGF)-A, -C, and -D, which exert their effects *via* tyrosine kinase receptors (VEGFRs). Angiogenic activity is promoted by VEGF-A mainly through VEGFR-2 (KDR/Flk-1). VEGFR-3 (Flt-4) and its primary ligand VEGF-C play dominant roles in lymphangiogenesis (8).

Citation: Journal of Oral Microbiology 2016, **8**: 32433 - http://dx.doi.org/10.3402/jom.v8.32433

Upon proteolytical activation, VEGF-C and -D bind to both VEGFR-2 and -3, exerting angiogenic as well as lymphangiogenic activity (9).

The presence of VEGFs and their receptors on osteoblasts and osteoclasts shows a link between vascular growth and bone turnover (10, 11). VEGF-C and -D appear to play a role in osteoclast differentiation and resorptive function *in vivo* through both VEGFR-2 and -3 (12). The VEGF signaling pathways have been incriminated in bone destructive processes such as cancer metastasis to bone, multiple myeloma, and rheumatoid arthritis (13–15).

Blood vessel endothelium and immune cells express VEGFs and VEGFRs in both rat and human periapical lesions. Their expression was seen in B- and T-cells, PMNs, as well as macrophages (16, 17). Osteoclasts were also found positive for VEGFR-2 and -3 in inflamed rat periapical tissue (17). However, neither in rat apical periodontium nor in human periapical lesions (16, 17) could lymphatic vessels be localized. Nevertheless, it has been shown that lymphangiogenesis occurs during development of marginal periodontitis, probably to enhance fluid and immune cell transport from the periphery toward the regional lymph nodes (18). Lymphadenitis can be observed in acute phases of apical periodontitis, demonstrating communication between the infected area and the local draining lymph nodes.

Recent studies on the role of VEGFR-2 and -3 in tumor progression and inflammation have tested the systemic blockade of VEGFR-2 and/or -3. Blocking of VEGFR-3 has increased the severity of inflammation in a mouse model of arthritis (19), while combined blockade of VEGFR-2 and -3 inhibited inflammatory lymphangiogenesis (20), angiogenesis, and tumor growth (21).

The aim of this study was to investigate the individual and combined roles of VEGFR-2 and -3 signaling with respect to periapical lesion size, inflammation, and angiogenesis by systemically blocking these receptors during induction of murine apical periodontitis. In addition, we investigated the inflammatory response in the draining regional lymph nodes of the same mice with respect to lymphangiogenesis and lymph node size.

Here we show that VEGFR-2 reduces, whereas combined VEGFR-2 and -3 signaling increases inflammation in murine apical periodontitis, independent of angiogenesis. We also demonstrate that lymphangiogenesis in the regional lymph nodes depends on either VEGFR-2 or -3 signaling.

Materials and methods

Animal experiments

A total of 74 male mice (C57BL/6 strain) were used, aged 8 weeks and weighing between 18–25 g. All mice were housed in polycarbonate cages, with no more than five animals per cage. They were fed standard pellet diet with tap water *ad libitum*. The experimental protocol was approved by the Regional Committee for Animal Research Ethics, University of Bergen, under the supervision of the Norwegian Experimental Animal Board.

Following 1 week to 10 days of acclimatization, the mice were anesthetized i.m. with a total of 0.2 mL mixture of ketamine 50 mg/mL, administered 100 mg/kg body weight (Ketalar®, Pfizer, NY), xylazine 20 mg/mL, administered 10 mg/kg body weight (Rompun Vet®, Bayer, Leverkusen, Germany), and sodium chloride (NaCl) 9 mg/mL, administered 0.12 mL/dosage. Mice assigned to treatment groups were then placed on a board to facilitate lower jaw retraction. Carbide burs sized 0.25 mm were used for pulp exposures of lower first molars performed under the operating microscope, avoiding perforation of the pulp chamber floor. Saline was used for irrigation. The mesial and distal root canals were then instrumented using a 0.06 K-file (Dentsply Maillefer, Ballaigues, Switzerland) and teeth were left open to the oral cavity for either 10 (28 mice) or 21 days (40 mice). The two observation periods were chosen in accordance with previous studies performed on rats showing active lesion development until day 15 and a chronic phase thereafter (22). All experiments were performed by a single operator.

Following dental operating procedures, the mice were divided in four groups for each observation period and injected intraperitoneal with either systemically blocking antibodies made in rat against mouse VEGFR-2 (anti-R2) (6.8 mg/mL DC101, Eli Lilly and Company, New York, NY, 140 μL/injection) and VEGFR-3 (anti-R3) (10.8 mg/mL, mF4-31C1, Eli Lilly and Company, 90 μL/injection). Groups 3 and 4 received combined VEGFR-2 and -3 treatment (anti-R2/R3) (6.8 mg/mL + 10.8 mg/mL, 230 μL/injection) and normal purified IgG rat anti-mouse (16.8 mg/mL, Europa Bioproducts, Cambridge, UK, 50 μL/injection), respectively. The injection protocols were applied in accordance with the company's recommendations and previous investigations (23, 24). Administrations were performed once per day at following intervals: day 0, 2, 4, 6, 9, 10 for the 10 days exposure groups; day 0, 2, 4, 6, 9, 12, 15, 18 for the 21 days exposure groups. The mice were subjected to gas anesthesia (Sevofluran, Baxter, Norway) provided *via* a face mask during the injection procedures. Six mice served as negative (non-exposed pulps and no antibody treatment) controls. Bilateral lower jaws and regional lymph nodes were collected from each mouse.

Micro-computed tomography imaging analysis and lesion size measurement

One randomly selected side of the 21 days exposed jaws from each group was fixed overnight in 4% paraformaldehyde (PFA). Thereafter, the jaws were washed with

Citation: Journal of Oral Microbiology 2016, **8**: 32433 - http://dx.doi.org/10.3402/jom.v8.32433

phosphate buffer, stored in 50% ethanol, number coded for blinded analysis, and sent for micro-computed tomography (μCT) evaluation to the Forsyth Institute, Cambridge, MA. The analysis was performed by means of a compact fan-beam-type tomograph (μCT40, Scanco Medical, Bassersdorf, Switzerland). The μCT system provides a 10 μm nominal resolution. The imaging parameters were as follows: tube voltage 70 kVp, current 140 μA, and integration time 300 ms. The data were exported into DICOM format and re-sliced in a standardized manner using the ImageJ (Wayne Rasband, National Institutes of Health, Bethesda, MD) software to obtain pivotal sections containing the entire length of the root canals and periapical lesions. The cross-sectional area of the periapical lesions on distal roots in mesiodistal as well as buccolingual directions was defined from the apical constriction to bone margins and measured by two independent observers in blinded images using Adobe Photoshop CS4 (Adobe Systems, San Jose, CA). The periapical lesions' sizes in mesio-distal directions were also measured in the 10 days groups on two to four immunohistochemically stained and blinded sections from each mouse, and values were averaged for each subject. A photomicroscope (Nikon Eclipse E600; Nikon Instruments, Kanagawa, Japan) connected to a digital camera employing NIS elements AR (Advanced Research) (Nikon Laboratory Imaging Software, Kanagawa, Japan) were used.

An averaged 25 μm^2 representing the normal periodontal ligament (PDL) size was subtracted from all recorded values. Results were expressed as squared millimeters (mm^2).

Protein extractions for Multiplex and ELISA analysis

Contralateral mandibles from all four 21 days groups ($n = 8$ in each group) and six samples from negative controls were used for protein extraction and further analysis. The tissue was rinsed with sterile phosphate buffered saline (PBS) and freed of clots and soft tissue. Periapical tissue from the first molars together with surrounding bone in a block specimen were carefully extracted under the surgical microscope and weighed. Thereafter, the samples were disrupted in a total volume of 400 μl cell lysis buffer (Cell Signaling Technology, Danvers, MA), supplemented with 1 mM phenylmethanesulfonyl fluoride (PMSF), Protease Inhibitor Cocktail (Cell Signaling Technology), and gentamicin 10 mg/mL (Sigma-Aldrich, St. Louis, MO). The supernatants were collected after centrifugation and subsequently frozen until further analysis.

For multiplex analysis of 25 cytokines using the 96-well Milliplex MAP mouse cytokine/chemokine magnetic bead panel (MCYTOMAG-70K, Millipore, MA), the samples were diluted 1:2 and incubated in duplicates with coupled beads. The panel included the following cytokines: granulocyte colony-stimulating factor (G-CSF), granulocyte-macrophage colony-stimulating factor (GM-CSF), IFN-γ, IL-1α, IL-1β, IL-2, IL-4, >IL-5, IL-6, IL-7, IL-9, IL-10, IL-12(p40), IL-12(p70), IL-13, IL-15, IL-17, interferon γ-induced protein-10 (IP-10), murine keratinocyte chemoattractant (MKC), monocyte chemoattractant protein-1 (MCP-1), macrophage inflammatory protein (MIP)-1α, MIP-1β, MIP-2, regulated on activation, normal T cell expressed and secreted (RANTES), and TNF-α.

Complexes were washed and incubated with detection antibody and thereafter with streptavidin–phycoerythrin. A range of 3.2–10.000 pg/mL recombinant cytokines was used to establish the standard curves. The levels of the inflammatory molecules were measured using a multiplex array reader from Luminex™ Instrumentation System (Bio-Plex Workstation from Bio-Rad Laboratories, Hercules, CA). The final concentrations were calculated using software provided by the manufacturer (Bio-Plex Manager Software).

For RANKL detection, samples were pipetted in duplicates on the TRANCE/RANKL/TNFSF11 (R&D Systems, Minneapolis, MN) kit using pre-coated plates. The assay uses the quantitative sandwich enzyme immunoassay (ELISA) technique. Upon adding the enzyme-linked polyclonal antibody specific to RANKL, a substrate solution is added, resulting in staining. The intensity of the color measured after stopping the reaction is proportional to cytokine concentration and the results are reported to a standard curve.

All cytokine or chemokine concentrations are calculated as pg/mg tissue corresponding to the samples' weight.

Immunohistochemical analysis and tartrate-resistant acid phosphatase staining of osteoclasts

PFA-fixed hemi-mandibles used for μCT scanning were decalcified in 10% EDTA, washed in phosphate buffer, and stored in sucrose at −80°C. Non-fixed frozen jaws exposed for 10 days were subjected to the same treatment prior to further analysis. Following serial cryosectioning at 12 μm thickness, two to four specimens from each mouse containing the region of interest – root canal and periapical lesion – were subjected to immunohistochemical analysis (IHC) analysis and tartrate-resistant acid phosphatase (TRAP) staining. All sections from the 10 days exposure groups were fixed on the glass with 4% PFA as a first step of the staining protocols.

TRAP was used for detection of osteoclasts and preosteoclasts using Leukocyte Acid Phosphatase for TRAP kit (Sigma-Aldrich St. Louis, MO), according to the manufacturer's instructions. In short, after fixation, selected slides were incubated in TRAP-staining buffer for 1 h at 37°C. Slides were rinsed for 10 min, counterstained with hematoxylin solution, and air-dried.

Adjacent sections were stained using the avidin–biotin peroxidase (ABC) method for identification of Ly-6.B2$^+$ neutrophils, F4/80$^+$ macrophages, and CD31$^+$ blood vessels, according to previously described protocols (16, 18).

Briefly, normal rabbit serum (Vector Laboratories Inc., Burlingame, CA) was used as blocking step, followed by primary antibodies overnight incubation at 4°C. Antigen-antibody complexes were evidenced by the ABC method, using a commercially available kit (Vectastain ABC kit; Vector Laboratories, Burlingame, CA), and visualized by 3, 3′-diaminobenzidine (DAB; Sigma-Aldrich Chemie GmbH, Steinheim, Germany) in the presence of 0.2% (w/v) ammonium nickel sulphate hydrate [$(NH_4)2Ni(SO_4)26H_2O$] to enhance the immunostaining. Finally, the sections were counterstained with methylene blue/azure II, dehydrated in graded alcohol series, cleared in xylene, and cover slipped with Eukitt (O. Kindler, Freiburg, Germany). Identification of VEGFR-2 and -3 in blood vessels, neutrophils, macrophages, and osteoclasts was performed by use of immunofluorescent double labeling with antibodies against VEGFR-2, VEGFR-3, CD31, Ly-6.B2, F4/80, calcitonin receptor, and cathepsin K. Osteoclasts expressing VEGFR-2 or -3 were stained with antibodies against calcitonin receptor and cathepsin K. The antibody–antigen complexes were visualized with Alexa Fluor −488/−594 secondary antibody conjugates (dilution 1:300, Invitrogen Corp., Carlsbad, CA). The presence of lymphatics in the periapical area was investigated by use of lymphatic vessel endothelial hyaluronan receptor-1 (LYVE-1) antibody. The employed antibodies were: Ly-6.B2 [rat anti-mouse, dilution 1:400 (DAB), 1:100 (immunofluorescent), AbD Serotec, Oxford, UK], F4/80 (rat anti-mouse, dilution 1:500, Acris, Herford, DE; dilution 1:50, Santa Cruz Biotechnology, Santa Cruz, CA, USA), VEGFR-2 (goat anti-mouse, dilution 1:20, Abcam, Cambridge, UK), VEGFR-3 (rabbit anti-mouse, dilution 1:100, Abcam), CD31 [rat anti-mouse, dilution 1:100 (DAB), 1:50 (immunofluorescent) AbD Serotec], calcitonin receptor (rabbit anti-mouse, dilution 1:20, Abcam), cathepsin K (goat anti-mouse, dilution 1:100, Santa Cruz Biotechnology), and LYVE-1 (rabbit anti-mouse, dilution 1:200, Abcam), respectively. The specificity of immune reactions was tested by omission of primary antibodies and/or substitution with isotype control. Fluorescent images were captured with a fluorescent microscope (Axio Imager; Carl Zeiss Microimaging Inc, Jena, Germany) connected to AxioCam MRm camera (Carl Zeiss) that used the AxioVision 4.8.1 (Carl Zeiss) imaging system. The periapical lesions on distal roots were outlined and the immunopositive cells and vessels within were quantified on two to four blinded sections from each mouse under a photomicroscope (Nikon Eclipse E600) connected to a digital camera using NIS elements AR imaging software and averaged for each animal.

Lymph node analysis

Upon serial cryosectioning (12–14 μm) of lymph nodes from all 21 days groups and six negative controls, every fourth section was fixed in 4% PFA and stained with H&E, and central regions were selected for total area measurements. Adjacent sections where the hilum area was prominent were chosen for fluorescent immunolabeling using primary antibody against LYVE-1 (dilution 1:200, Abcam) and Alexa Fluor 546 conjugated secondary antibody (dilution 1:300, Invitrogen Corp.) for visualization of the antigen–antibody complexes. Fluorescent images were captured with a fluorescent microscope (Axio Imager) that used the AxioVision 4.8.1 (Carl Zeiss) imaging system. Sections stained with H&E were visualized under photomicroscope (Nikon Eclipse E600) using NIS elements AR imaging software. All further image quantification was performed with the same software. Total area of each lymph node was outlined and measured at 4× magnification. The results, presented in mm^2, denote lymph node sizes. Lymphatic sinus LYVE-1^+ areas were measured in hilum and medulla in a grid representing 350 × 350 μm in blinded sections. Lymph node sizes and area fraction measurements were calculated in four to six sections from each mouse.

Statistical analyses

All data was subjected to statistical analysis using the GraphPad Prism 5 Software (GraphPad, San Diego, CA). Multiple groups comparisons have been carried out and the following tests were used: one-way ANOVA and Bonferroni post-hoc test for normally distributed populations; Kruskal–Wallis and Dunn's post-hoc test for non-normally distributed populations; two-way ANOVA and Bonferroni post-hoc test for grouped analysis. p value of <0.05 was considered statistically significant.

Results

Blood vessels, immune cells, and osteoclasts expressed VEGFR-2 and -3, whereas no lymphatic vessels were found in periapical lesions

Double immunofluorescent staining was used to identify the sources of VEGFR-2 and -3 in periapical lesions from IgG-treated mice. $CD31^+$ blood vessels and immune cells expressed both VEGFR-2 and -3 (Fig. 1A and B). Ly-$6.B2^+$ neutrophils and $F4/80^+$ macrophages were found to express VEGFR-2 and -3 in inflamed apical PDL, as exemplified in Fig. 1C and D. Osteoclasts identified with calcitonin receptor or cathepsin K were also VEGFR-2 and -3 positive (Fig. 1E and F). No LYVE-1^+ lymphatic vessels were found in the periapical area (data not shown).

Lesions expanded faster after blocking of either VEGFR-2 or -3

All mice developed periapical lesions upon pulpal exposure, shown in Fig. 2A and B. An initial substantial increase in lesion sizes was observed in the anti-R2 and anti-R3 groups following 10 days of exposure, larger than

Citation: Journal of Oral Microbiology 2016, 8: 32433 - http://dx.doi.org/10.3402/jom.v8.32433

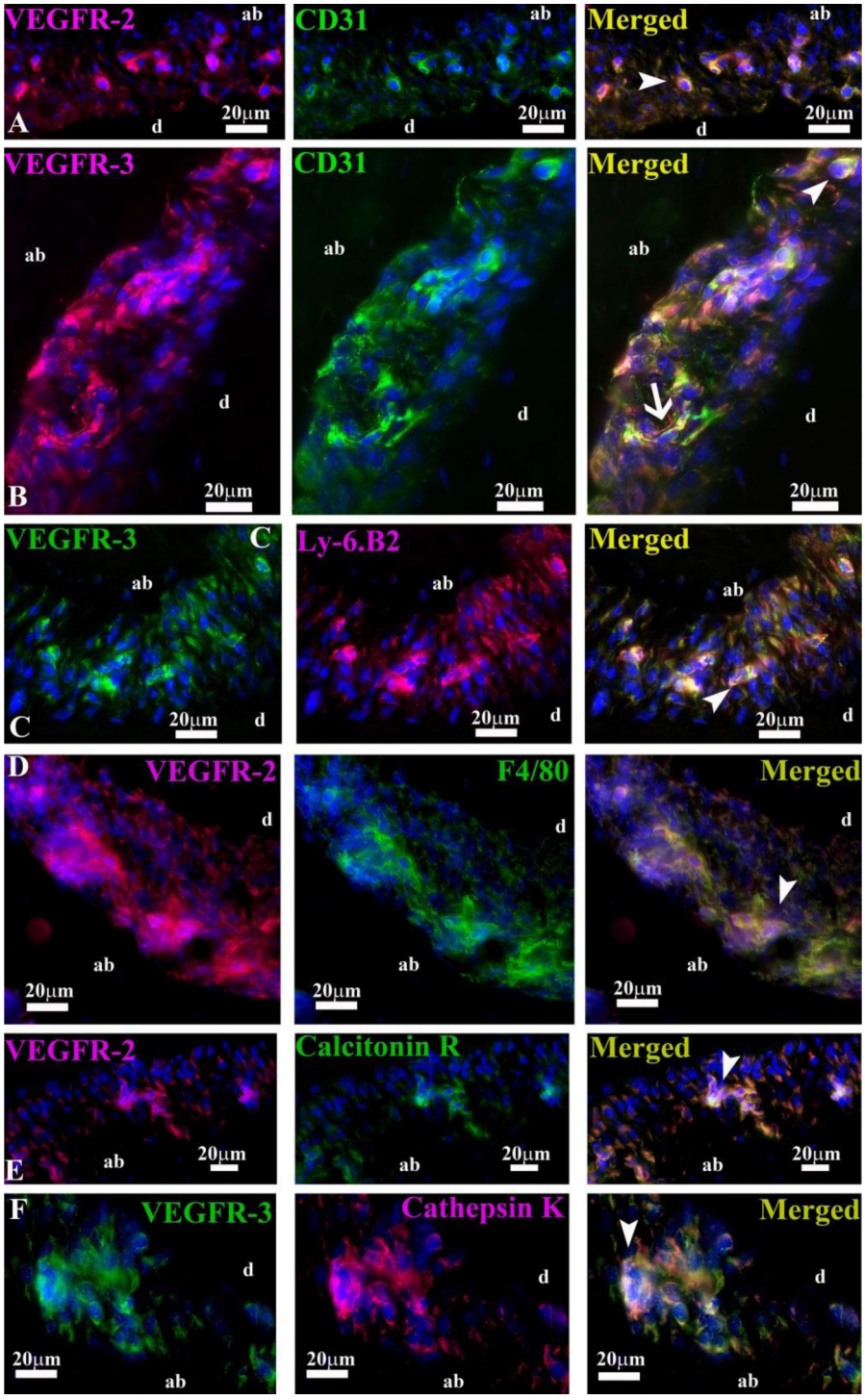

Fig. 1. Immune cells, blood vessels, and osteoclasts are VEGFR-2 and -3 positive in inflamed apical periodontium. $CD31^+$ immune cells (arrowheads) and blood endothelial cells (arrow) express VEGFR-2 (A) and VEGFR-3 (B), respectively. Ly-$6.B2^+$ neutrophils (C) and $F4/80^+$ macrophages (D) (arrowhead) exhibit VEGFR-2 and -3. $VEGFR\text{-}2^+$ (E) and $VEGFR\text{-}3^+$ (F) osteoclasts (arrowhead) were identified with antibodies against calcitonin receptor and cathepsin K. All sections are from IgG-treated animals (ab, alveolar bone; d, dentin).

in the IgG and anti-R2/R3 groups. From day 10 to 21, only a modest non-significant lesion expansion was seen in the anti-R2 and anti-R3 groups. This indicates that a plateau phase was reached already by day 10 in these groups. In contrast, the IgG and anti-R2/R3 groups reached the same level first after 21 days, with

Fig. 2. Periapical bone resorption upon endodontic infection in first mandibular molars. Lesion sizes were measured on the distal roots in immunohistochemically stained sections on day 10 (A) and in µCT sections on day 21 (B). The periapical lesion, marked in red, is measured with use of a standard template placed on the apical constriction and outlined to the peripheral bone margins. Normal PDL width can be seen in the second, non-exposed molar of the exemplified µCT section. Lesion sizes showed a slower progression from day 0 to day 10 in the anti-R2/R3 and IgG compared with the anti-R2 or anti-R3 groups, but increased significantly within all experimental groups. From day 10 to day 21 the lesion growth was significant only within the IgG and anti-R2/R3 groups (C). $*p < 0.05$, $**p < 0.005$.

a statistically significant increase in lesion size between the two observation periods only within the groups (Fig. 2C).

Pro-inflammatory cytokines were upregulated after anti-R2 treatment and downregulated after anti-R2/R3 treatment

To determine the level of local inflammation in the apical area, we measured a panel of cytokine levels. The multiplex analysis revealed that 18 of 25 tested cytokines were expressed in the periapical tissues of all experimental groups. IL-15 was significantly upregulated already after 10 days in the anti-R2 group compared with IgG controls. At day 21, the pro-inflammatory cytokines IL-1α, IL-1β, RANTES, TNF-α, IL-15, IL-17, IFN-γ, and MCP-1 showed the highest values in the anti-R2 group, however not significant when compared with the IgG group. In the anti-R2/R3 group, a tendency to downregulation of some cytokines was observed on day 21 for IL-17, RANKL, MCP-1, IL-6, MIP-1α, MIP-1β, MIP-2, GM-CSF, and IP-10, statistically significant for IL-17, MCP-1, MIP-1β, and RANKL compared with the IgG group (Fig. 3).

Recruitment of neutrophils and number of TRAP$^+$ osteoclasts were enhanced after anti-R2 treatment, while R2/R3 blocking hampered mobilization of macrophages after 10 days of pulp exposure

Following the spread of infection down the root canal, immune cells are recruited into the apical area and osteoclasts are activated. We therefore counted the number of different immune cells and osteoclasts apically in each group. The number of TRAP$^+$ osteoclasts and Ly-6.B2$^+$ neutrophils increased significantly in the anti-R2 group compared with the other test groups on day 10 (Fig. 4A–F). Following 3 weeks of pulp exposure, extensive Ly-6.B2$^+$ cellular infiltration was seen in both the anti-R2 and anti-R3 groups, yet only significant compared with the anti-R2/R3 group ($p < 0.05$) (Fig. 4F).

Significantly fewer F4/80$^+$ macrophages were recorded in the anti-R2/R3 group after 10 days compared with IgG controls and with all experimental groups, respectively ($p < 0.05$) (Fig. 4G–I).

On day 21, big resorptive lesions with discontinuous and indistinct peripheral bone delimitation were found in all experimental groups, and hence the TRAP$^+$ cells quantitation was left out at this observation period.

Induced angiogenesis during periapical lesion formation is inhibited by VEGFR-2 and combined VEGFR-2 and -3 blocking

A hallmark of inflammation is angiogenesis, a process known to be influenced by VEGF signaling. Number of CD31$^+$ vessels is indicative of angiogenic activity. Angiogenesis took place in the IgG and anti-R3 groups at both observation times when compared with normal PDL. Ten days after pulp exposures, significantly fewer CD31$^+$ vessels were counted in the anti-R2/R3 group ($p < 0.05$), showing vessel density in the lesions similar to normal PDL. The angiogenic activity was abolished in both the anti-R2 and anti-R2/R3 groups on day 21 (Fig. 4J–L).

Lymphangiogenesis in the cervical lymph nodes is prevented by blocking of VEGFR-2 or -3, whereas lymph node size is increased after anti-R2 treatment

As the inflammation is spread from the dental area to the lymph nodes *via* lymph, we investigated lymphangiogenesis in the draining lymph nodes in each group of mice after 21 days of exposure.

Lymph node sizes increased significantly upon VEGFR-2 blocking when compared with negative controls and the anti-R2/R3 group (Fig. 5A). The LYVE-1$^+$ area fraction in the lymph nodes hilum and medulla was

Citation: Journal of Oral Microbiology 2016, **8**: 32433 - http://dx.doi.org/10.3402/jom.v8.32433

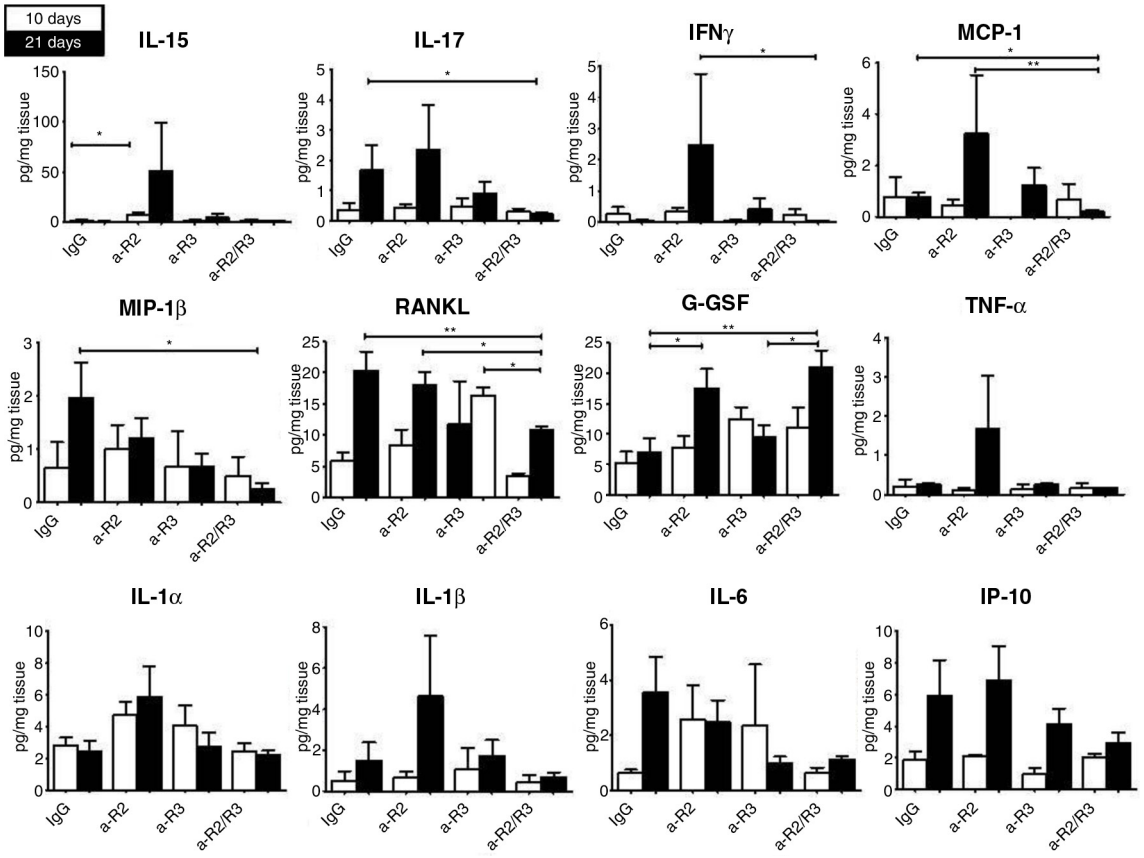

Fig. 3. Graphs represent cytokines and chemokines expression as found in periapical lesions after 10 (in white) and 21 days (in black) observation time. IL-15 exhibited a significant increase at day 10 in the anti-R2 group when compared with IgG controls. Other pro-inflammatory cytokines, such as IL-17, MIP-1β, MCP-1, and RANKL, showed a significant downregulation after anti-R2/R3 treatment at day 21. In contrast, G-CSF significantly increased after combined R2/R3 treatment. Other cytokines showed a general tendency to increased expression after anti-R2 treatment. Cytokines expression were measured with multiplex/ELISA methods and are presented as means with SEM (SEM, standard error of the mean; a, anti.). Horizontal bars point at statistically significant differences. *$p < 0.05$, **$p < 0.001$. Of technical reasons only two samples were analyzed in the anti-R3 group at day 10.

greater in the IgG-treated group compared with the other groups, yet only significant in the medulla ($p < 0.05$) (Fig. 5B–E).

Discussion

The major findings of the present study were: 1) blocking of VEGFR-2 resulted in increased periapical inflammation observed as increased recruitment of neutrophils and activation of osteoclasts, a tendency to increased pro-inflammatory cytokine levels, along with a more rapid lesion development; 2) combined inhibition of VEGFR-2 and -3 signaling reduced the apical inflammatory responses after pulp exposure seen as diminished macrophage recruitment and a decreased level of pro-inflammatory cytokines; 3) lymphangiogenesis in the draining lymph nodes is equally dependent on VEGFR-2 and -3.

We hereby confirm that both VEGFR-2 and -3 are expressed on blood vessels, immune cells, and osteoclasts in mouse apical periodontitis (Fig. 1), as previously shown in human and rat lesioned apical area (16, 17). Blocking of VEGFR-2 and a combined inhibition of VEGFR-2 and -3 impaired angiogenesis, while inhibiting VEGFR-3 alone had no effect on the growth of blood vessels in the lesions. The findings demonstrate the dominant role of VEGFR-2 signaling in angiogenesis, but the overall results indicate that the elevated inflammatory response in the anti-R2 group is independent of angiogenesis.

In a model of corneal inflammation, combined systemic blocking of VEGFR-2 and -3 inhibited inflammatory lymphangiogenesis, along with a reduction of angiogenesis (20). We observed reduced angiogenesis in the apical area after the same systemic treatment, but lymphatic vessels were missing from the apical periodontium, as also seen in human and rat periapical lesions (16, 17).

Systemic inhibition of VEGFR-2 resulted in decreased severity of arthritis and skin inflammation (19, 24), in contrast with our findings where the apical inflammation became more severe after VEGFR-2 blocking, especially

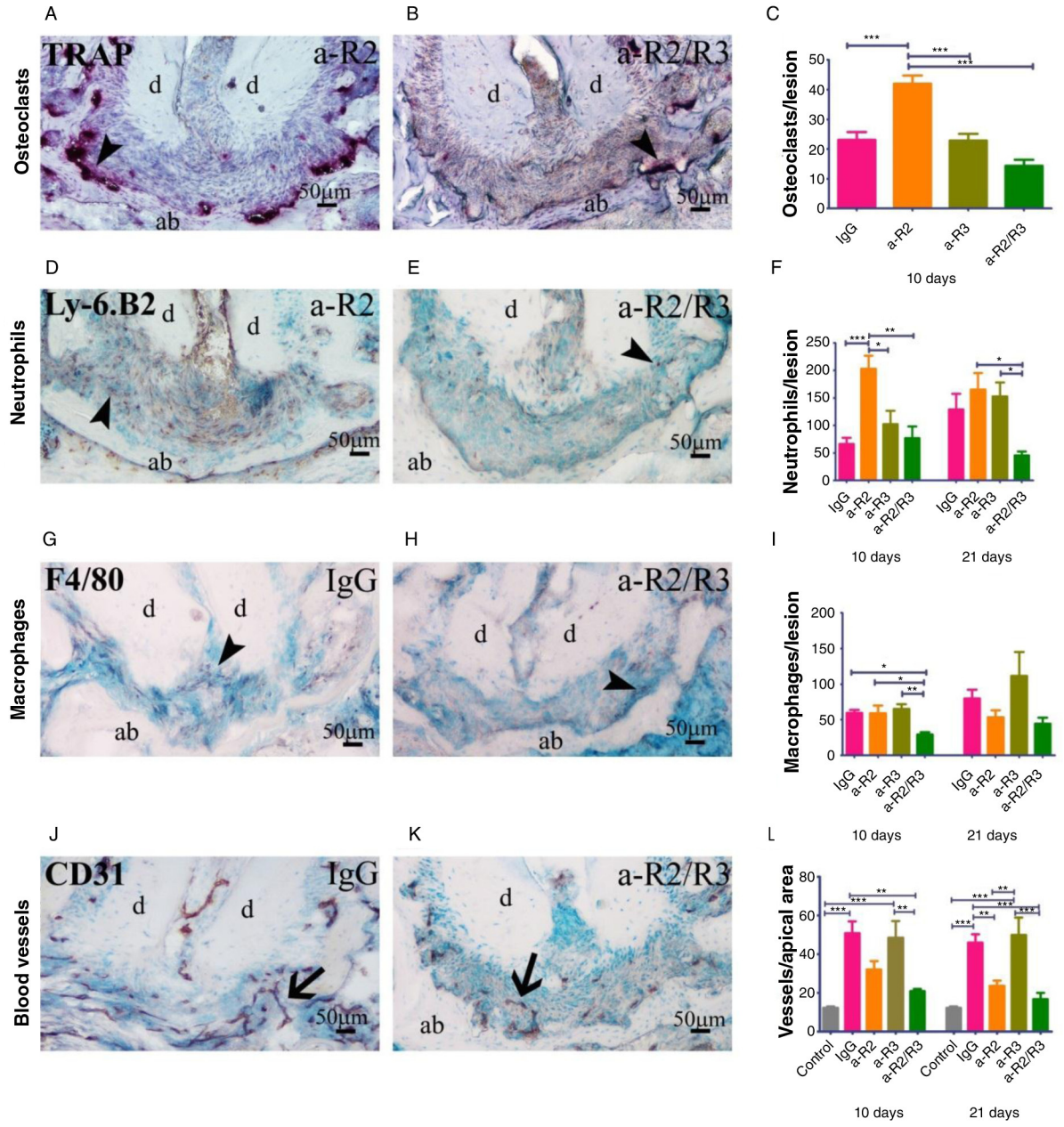

Fig. 4. Quantification of osteoclasts, immune cells, and blood vessels in periapical lesions. TRAP$^+$ osteoclasts (arrowheads) are demonstrated in sections from an anti-R2 (A) and an anti-R2/R3 (B) treated mouse at day 10. Their numbers significantly increased in the anti-R2 group (C). Immunostaining of Ly-6.B2$^+$ neutrophils (arrowheads) in the apical area at day 10 in an anti-R2 treated mouse (D) illustrating increased PMN infiltrate when compared with anti-R2/R3 treated animal (E). The anti-R2 group of mice exhibited the highest amounts of PMN cells in the apical area compared with all other experimental groups at day 10 (F). F4/80$^+$ macrophages (arrowheads) are shown in the IgG group (G) and the anti-R2/R3 group (H) at day 10. Significantly fewer macrophages were observed in the anti-R2/R3 group 10 days after pulp exposure, compared with all other experimental groups, maintaining a similar tendency on day 21 (I). CD31$^+$ blood vessels (arrows) from the IgG group (J) and the anti-R2/R3 group (K) exemplified at day 10. Angiogenesis was observed in the IgG and anti-R3 groups, and was inhibited in the anti-R2 and anti-R2/R3 groups (L). All graphs represent means with SEM (SEM, standard error of the mean; a, anti; d, dentin; ab, alveolar bone). Horizontal bars point at statistically significant differences. *$p < 0.05$, **$p < 0.005$, ***$p < 0.0001$.

during the active development stage. In arthritis and skin inflammation, lymphangiogenesis is induced and is affected by both VEGFR-2 and -3 inhibition (24–26), whereas in the apical area no lymphatic vessels were found. The signaling of VEGFR-2 and -3 in the apical area takes place in blood vessels and in immune cells only, and may explain the contradictory results. Another difference is the infectious origin of our investigated inflam-

Citation: Journal of Oral Microbiology 2016, **8**: 32433 - http://dx.doi.org/10.3402/jom.v8.32433

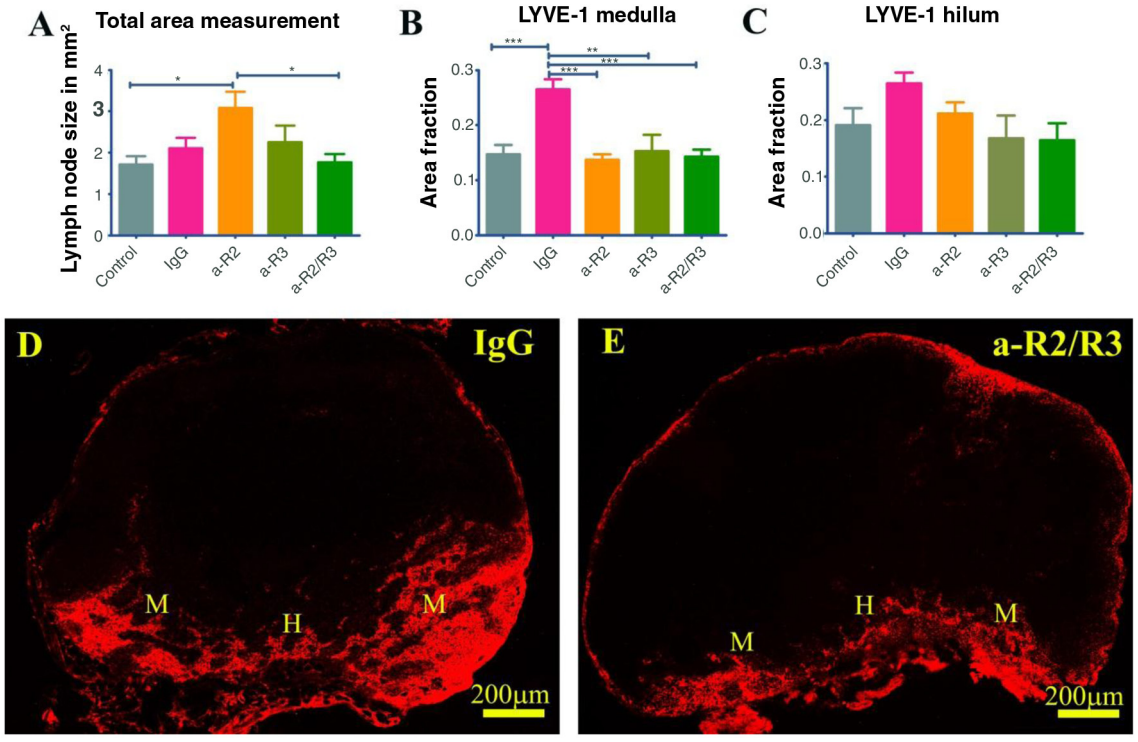

Fig. 5. Measurements of draining lymph nodes (LN) size and lymphangiogenesis after 21 days of pulp exposure. The LN sizes (A) given as total area measurements (mm^2) showed the largest values in the anti-R2 group. Area fraction measurements (LYVE-1^+ area/pre-delimited grids of 350×350 µm) of lymphatics in medulla (B) and hilum (C) showed that lymphangiogenesis was inhibited in all VEGFR-blocking groups compared with IgG controls and was significantly lower in the medulla (B). Images show LYVE-1^+ areas in hilum and medulla of the IgG group (D) and the anti-R2/R3 group (E). All values represent means with SEM (SEM, standard error of the mean; a, anti; M, medulla; H, hilum). Horizontal bars point at statistically significant differences. $*p < 0.05$, $**p < 0.005$, $***p < 0.0001$.

matory process. In contrast, arthritis and chronic skin inflammation models are both sterile inflammations.

Blockade of VEGFR-2 or -3 signaling pathways prevented lymph node enlargement in a model of TNF-transgenic mice which developed spontaneous arthritis (19). In the current study, draining lymph node lymphangiogenesis is equally dependent on VEGFR-2 and -3 signaling as the individual blocking of both receptors inhibited lymphangiogenesis. The finding is in line with other studies on inflammatory lymphangiogenesis (20, 27). Inflammatory response in the regional lymph nodes measured as lymph node size was significantly increased after anti-R2 treatment compared with negative controls alone, and probably reflects the strong inflammatory response seen in the apical area in this group of animals. Transport of antigens, either by immune cells or by soluble and inflammatory mediators, must be carried in lymphatic vessels to the lymph nodes, where they induce an inflammatory response. However, localization of the uptake of fluid and immune cells from the apical area into lymphatics is hitherto unknown.

In the current study, periapical lesions after 10 days observation time show a tendency to an increased size in the anti-R2 and anti-R3 groups compared with IgG and anti-R2/R3 treatments. In the anti-R2 group, the results probably reflect the stronger inflammatory response seen in this population and expressed as a significantly increased number of $TRAP^+$ osteoclasts and $Ly6B2^+$ neutrophils. In the anti-R3 group, the explanation of initial fast lesion expansion may be a direct VEGFR-3 effect on osteoclasts which does not affect cellular numbers but their resorptive activity. VEGFR-3 is known to be expressed on these cells in apical lesions (17), and that has also been shown in the current investigation. The fact that both VEGFR-2 and -3 are expressed in immune cells, blood vessels, and osteoclasts in the apical area (16, 17) makes it difficult to conclude whether responses observed after blocking of the receptors are due to direct and/or indirect effects.

Neutrophils are the first line of defense in apical periodontitis. They attract and stimulate other PMNs and macrophages. By releasing different enzymes and cytokines, PMNs contribute to both the elimination of bacteria, as well as host tissue destruction. IL-15 is known to induce cell proliferation of natural killer cells and maturation of macrophages (28). IL-15 has also been shown to upregulate IFN-γ level by PMNs (29) and both cytokines were upregulated in the anti-R2 group.

IL-15 already exhibits an upregulation on day 10 in this group of experimental animals.

Individual inhibitions of either VEGFR-2 or -3 do not result in any difference regarding macrophage amounts during the active lesion development compared with IgG controls. However, the combined treatment appears to constrain macrophage recruitment. This may explain the low expression of pro-inflammatory cytokines, seen already from day 10 of pulp exposure in this experimental group.

Increased expression of IL-17, IFN-γ, and RANKL are all linked to bone resorptional activity (30), and are all cytokines that showed a significant decrease after combined R2/R3 blockade compared with IgG controls in the current investigation. MCP-1 is the main chemokine for monocyte recruitment and has been implicated in a variety of inflammatory diseases, such as rheumatoid arthritis or atherosclerosis (31, 32). MCP-1 is also involved in the development and function of osteoclasts. It was stated that RANKL can induce MCP-1 expression (33), accelerating the osteoclastic differentiation *via* autocrine pathways. Under the current experimental conditions, MCP-1 along with RANKL showed a significantly decreased expression after combined VEGFR-2 and -3 inhibition. In multiple myeloma osteolytic lesions, MIP-1α and -1β have been described as potent osteoclastogenic chemokines, a process which occurs *via* RANKL (34). Both MIP-1α and -1β show similar expression patterns in the current investigation of murine apical periodontitis; however, only MIP-1β exhibits a significant decrease after combined R2/R3 blockade.

G-CSF usually augments the production and modulates the differentiation of neutrophils and is also involved in monocyte/macrophage expansion, enhancement of phagocytic function, and the regulation of inflammatory cytokine and chemokine production (35, 36). Contrary to initial beliefs, G-CSF has beneficial roles during inflammatory conditions (36) and seems to downregulate LPS-induced TNF-α expression (37). Under the experimental conditions of this study, G-CSF increased significantly in well-established periapical lesions upon both VEGFR-2 and combined VEGFR-2 and -3 blocking. The latter finding supports the previously described anti-inflammatory effect of G-CSF and, along with the low expression of earlier discussed pro-inflammatory cytokines in the same group of animals, points at an anti-inflammatory outcome of R2/R3 inhibition.

The exact mechanism on how VEGFR-2 signaling prevents whereas simultaneous signaling of VEGFR-2 and -3 enhances the inflammatory response in the apical area is unknown and in need of further investigation.

Conclusions

We demonstrate an anti-inflammatory effect of VEGFR-2 along with a pro-inflammatory effect of combined VEGFR-2 and -3 signaling in periapical lesions. The effects seem to involve neutrophil regulation and are independent of angiogenesis. In the cervical lymph nodes, lymphangiogenesis is seen after pulp exposure and is promoted through activation of VEGFR-2 and/or VEGFR-3.

Acknowledgements

We thank Åse Rye Eriksen and Pål William Wallace, Department of Biomedicine, University of Bergen for technical assistance and Bronislaw Pytowski and Eli Lilly and Company, New York, NY, US for providing the antibodies against VEGFR-2 and -3.

Conflict of interest and funding

Financial support received from Helse Vest, Norway, project number 911684 and from the University of Bergen. There is no conflict of interest in the present study for any of the authors.

References

1. Stashenko P, Teles R, D'Souza R. Periapical inflammatory responses and their modulation. Crit Rev Oral Biol 1998; 9: 498–521.
2. Gilles JA, Carnes DL, Dallas MR, Holt SC, Bonewald LF. Oral bone loss is increased in ovariectomized rats. J Endod 1997; 23: 419–22.
3. Jiang Y, Mehta CK, Hsu TY, Alsulaimani FF. Bacteria induce osteoclastogenesis via an osteoblast-independent pathway. Infect Immun 2002; 70: 3143–8.
4. Graves DT, Oates T, Garlet GP. Review of osteoimmunology and the host response in endodontic and periodontal lesions. J Oral Microbiol 2011; 3: 5304, doi: http://dx.doi.org/10.3402/jom.v3i0.5304
5. De Rossi A, Rocha LB, Rossi MA. Interferon-gamma, interleukin-10, intercellular adhesion molecule-1, and chemokine receptor 5, but not interleukin-4, attenuate the development of periapical lesions. J Endod 2008; 34: 31–8.
6. Huang GT, Do M, Wingard M, Park JS, Chugal N. Effect of interleukin-6 deficiency on the formation of periapical lesions after pulp exposure in mice. Oral Surg Oral Med Oral Pathol Oral Radiol Endod 2001; 92: 83–8.
7. Halin C, Detmar M. Chapter 1. Inflammation, angiogenesis, and lymphangiogenesis. Methods Enzymol 2008; 445: 1–25.
8. Tammela T, Alitalo K. Lymphangiogenesis: molecular mechanisms and future promise. Cell 2010; 140: 460–76.
9. Anisimov A, Alitalo A, Korpisalo P, Soronen J, Kaijalainen S, Leppänen V-M, et al. Activated forms of VEGF-C and VEGF-D provide improved vascular function in skeletal muscle. Circulation Res 2009; 104: 1302–12.
10. Tombran-Tink J, Barnstable CJ. Osteoblasts and osteoclasts express PEDF, VEGF-A isoforms, and VEGF receptors: possible mediators of angiogenesis and matrix remodeling in the bone. Biochem Biophys Res Commun 2004; 316: 573–9.
11. Marini M, Sarchielli E, Toce M, Acocella A, Bertolai R, Ciulli C, et al. Expression and localization of VEGF receptors in human fetal skeletal tissues. Histol Histopathol 2012; 27: 1579–87.
12. Motokawa M, Tsuka N, Kaku M, Kawata T, Fujita T, Ohtani J, et al. Effects of vascular endothelial growth factor-C and -D on osteoclast differentiation and function in human peripheral blood mononuclear cells. Arch Oral Biol 2013; 58: 35–41.
13. Aldridge SE, Lennard TW, Williams JR, Birch MA. Vascular endothelial growth factor acts as an osteolytic factor in breast cancer metastases to bone. Br J Cancer 2005; 92: 1531–7.

14. Hah YS, Jun JS, Lee SG, Park BW, Kim DR, Kim UK, et al. Vascular endothelial growth factor stimulates osteoblastic differentiation of cultured human periosteal-derived cells expressing vascular endothelial growth factor receptors. Mol Biol Rep 2011; 38: 1443–50.
15. Sosnoski DM, Krishnan V, Kraemer WJ, Dunn-Lewis C, Mastro AM. Changes in cytokines of the bone microenvironment during breast cancer metastasis. Int J Breast Cancer 2012; 2012: 160265.
16. Virtej A, Loes SS, Berggreen E, Bletsa A. Localization and signaling patterns of vascular endothelial growth factors and receptors in human periapical lesions. J Endod 2013; 39: 605–11.
17. Bletsa A, Virtej A, Berggreen E. Vascular endothelial growth factors and receptors are up-regulated during development of apical periodontitis. J Endod 2012; 38: 628–35.
18. Mkonyi LE, Bletsa A, Bolstad AI, Bakken V, Wiig H, Berggreen E. Gingival lymphatic drainage protects against *Porphyromonas gingivalis*-induced bone loss in mice. Am J Pathol 2012; 181: 907–16.
19. Guo R, Zhou Q, Proulx ST, Wood R, Ji RC, Ritchlin CT, et al. Inhibition of lymphangiogenesis and lymphatic drainage via vascular endothelial growth factor receptor 3 blockade increases the severity of inflammation in a mouse model of chronic inflammatory arthritis. Arthritis Rheum 2009; 60: 2666–76.
20. Yuen D, Pytowski B, Chen L. Combined blockade of VEGFR-2 and VEGFR-3 inhibits inflammatory lymphangiogenesis in early and middle stages. Invest Ophthalmol Vis Sci 2011; 52: 2593–7.
21. Tammela T, Zarkada G, Wallgard E, Murtomäki A, Suchting S, Wirzenius M, et al. Blocking VEGFR-3 suppresses angiogenic sprouting and vascular network formation. Nature 2008; 454: 656–60.
22. Stashenko P, Wang C, Tani-Ishii N, Yu S. Pathogenesis of induced rat periapical lesions. Oral Surg Oral Med Oral Pathol 1994; 78: 494–502.
23. Baluk P, Tammela T, Ator E, Lyubynska N, Achen MG, Hicklin DJ, et al. Pathogenesis of persistent lymphatic vessel hyperplasia in chronic airway inflammation. J Clin Invest 2005; 115: 247–57.
24. Huggenberger R, Ullmann S, Proulx ST, Pytowski B, Alitalo K, Detmar M. Stimulation of lymphangiogenesis via VEGFR-3 inhibits chronic skin inflammation. J Exp Med 2010; 207: 2255–69.
25. Zhang Q, Lu Y, Proulx S, Guo R, Yao Z, Schwarz E, et al. Increased lymphangiogenesis in joints of mice with inflammatory arthritis. Arthritis Res Ther 2007; 9: R118.
26. Polzer K, Baeten D, Soleiman A, Distler J, Gerlag D, Tak P, et al. Tumour necrosis factor blockade increases lymphangiogenesis in murine and human arthritic joints. Ann Reheum Dis 2008; 67: 1610–16.
27. Liu ZY, Qiu HO, Yuan XJ, Ni YY, Sun JJ, Jing W, et al. Suppression of lymphangiogenesis in human lymphatic endothelial cells by simultaneously blocking VEGF-C and VEGF-D/VEGFR-3 with norcantharidin. Int J Oncol 2012; 41: 1762–72.
28. Ohteki T. Critical role for IL-15 in innate immunity. Curr Mol Med 2002; 2: 371–80.
29. Rodrigues DR, Fernandes RK, Balderramas Hde A, Penitenti M, Bachiega TF, Calvi SA, et al. Interferon-gamma production by human neutrophils upon stimulation by IL-12, IL-15 and IL-18 and challenge with *Paracoccidioides brasiliensis*. Cytokine 2014; 69: 102–9.
30. Araujo-Pires AC, Biguetti CC, Repeke CE, Rodini Cde O, Campanelli AP, Trombone AP, et al. Mesenchymal stem cells as active prohealing and immunosuppressive agents in periapical environment: evidence from human and experimental periapical lesions. J Endod 2014; 40: 1560–5.
31. Hayashida K, Nanki T, Girschick H, Yavuz S, Ochi T, Lipsky PE. Synovial stromal cells from rheumatoid arthritis patients attract monocytes by producing MCP-1 and IL-8. Arthritis Res 2001; 3: 118–26.
32. Kusano KF, Nakamura K, Kusano H, Nishii N, Banba K, Ikeda T, et al. Significance of the level of monocyte chemoattractant protein-1 in human atherosclerosis. Circ J 2004; 68: 671–6.
33. Kim MS, Day CJ, Morrison NA. MCP-1 is induced by receptor activator of nuclear factor-{kappa}B ligand, promotes human osteoclast fusion, and rescues granulocyte macrophage colony-stimulating factor suppression of osteoclast formation. J Biol Chem 2005; 280: 16163–9.
34. Abe M, Hiura K, Wilde J, Moriyama K, Hashimoto T, Ozaki S, et al. Role for macrophage inflammatory protein (MIP)-1alpha and MIP-1beta in the development of osteolytic lesions in multiple myeloma. Blood 2002; 100: 2195–202.
35. Fattorossi A, Battaglia A, Pierelli L, Malinconico P, Andreocci L, Perillo A, et al. Effects of granulocyte-colony-stimulating factor and granulocyte/macrophage-colony-stimulating factor administration on T cell proliferation and phagocyte cell-surface molecules during hematopoietic reconstitution after autologous peripheral blood progenitor cell transplantation. Cancer Immunol Immunother 2001; 49: 641–8.
36. Xu S, Höglund M, Hâkansson L, Venge P. Granulocyte colony-stimulating factor (G-CSF) induces the production of cytokines *in vivo*. Brit J Haematol 2000; 108: 848–53.
37. Gorgen I, Hartung T, Leist M, Niehorster M, Tiegs G, Uhlig S, et al. Granulocyte colony-stimulating factor treatment protects rodents against lipopolysaccharide-induced toxicity via suppression of systemic tumor necrosis factor-alpha. J Immunol 1992; 149: 918–24.